Dispersion manipulation in optical coherence tomography with Fourier-domain optical delay line

A. Ceyhun Akcay[*], Kye-sung Lee, Jannick. P. Rolland

College of Optics and Photonics: CREOL & FPCE, University of Central Florida,
4000 Central Florida Blvd., Orlando FL 32816

ABSTRACT

In the last decade, Fourier-domain optical delay lines (FD-ODL) based on pulse shaping technology have emerged as a practical device for high-speed scanning and dispersion compensation in imaging interferometry such as optical coherence tomography(OCT). In this study, we investigate the effect of first- and second-order dispersion on the photocurrent signal associated with a fiber-optic OCT system implemented using a superluminescent diode centered at 950nm±35nm, an FD-ODL, and a mirror and a layered $LiTaO_3$ which owns suitable dispersion characteristics to model a skin specimen. We present a practically useful method associated with FD-ODL to minimize the effect of dispersion through the OCT system and the specimen combined, and quantify the results using two general metrics for axial resolution.

Keywords: Fourier-domain optical delay line, optical coherence tomography, dispersion compensation

1. Introduction

Fiber-optic imaging interferometers such as employed in OCT have been developed to image internal structures of biological tissues and other turbid materials accurately, rapidly, and noninvasively by use of the partial temporal coherence of a broadband light source.[1-3] Because of the broadband nature of the light source, dispersion is an important issue in imaging interferometry, as the fiber optics, the specimen, and other dispersive components may induce significant dispersion. A dispersion mismatch between the interferometer arms affects the temporal width and shape of the photocurrent signal and consequently affects the longitudinal resolution of the imaging system. Therefore, balancing dispersion between the reference and the specimen arms is necessary to achieve the highest possible axial resolution throughout the imaging depth of the specimen.

There are two approaches to compensate dispersion: One is a post-imaging digital technique such as numerical dispersion compensation, the other is a pre-imaging optical technique. Within post-imaging compensation, numerical algorithms based on the fast Fourier transform[4] or the numerical correlation of the depth scan signal with a depth variant kernel[5] were presented for computationally correcting the effect of material dispersion on OCT signal data. An autofocus algorithm was also presented for rapid image correction.[6] Recently, other numerical methods based on Fourier transform techniques were adopted to compensate dispersion in spectral domain OCT by correcting the frequency-dependent nonlinear phase of the received spectral OCT signal.[7,8,9] Within pre-imaging compensation, optical dispersion balancing between the specimen and the reference arms is typically achieved by placing a dispersive optical element, such as a pair of prisms employed as a variable thickness dispersive plate in the reference arm. More recently, a Fourier-domain optical delay line (FD-ODL) was presented for dispersion compensation.[10] The FD-ODL was first introduced for high-speed scanning[11,12] and proposed for the potential assessment of dispersion in the sample.[13]

In this paper, we derive the photocurrent signal function in the interferometer accounting for up to second-order dispersion, together with an experimental validation of the theoretical predictions. Furthermore, we propose a practically useful optical method using an FD-ODL to minimize the broadening effect of first-order dispersion and

---
[*] akcay@creol.ucf.edu; Phone: 407-823-6853; Fax: 407-823-6880

asymmetry of second-order dispersion on the point spread function (PSF) throughout a layered material. The method is experimentally demonstrated for a layered $LiTaO_3$ material having a similar dispersion at 950nm as a skin specimen.

The schematic diagram of an OCT system associated with an FD-ODL in the reference arm of the fiber optic interferometer is shown in Figure 1. A collimated beam is incident on a diffraction grating and dispersed spatially. After propagating through the lens, the light is then projected on a tiltable mirror. The pivot point of the mirror may be offset from the optical axis by a distance x_0. The reflected, dispersed light is focused back onto the grating through the lens and then reflected by a double-pass mirror. The double-pass mirror returns the light to the collimator through the same path the light propagated. The dispersion introduced by the FD-ODL in the reference arm of the fiber optic interferometer can be controlled by the grating axial shift Δz from the focal plane of the lens, as well as the tilt angle θ_g of the grating normal with respect to optical axis of the FD-ODL.[14] Therefore, the grating axial shift and tilt angle have an effect on the axial point spread function, which is the envelope of the interferometric autocorrelation of the optical field reflected from the specimen and the optical field reflected from the reference mirror of the FD-ODL. Consequently, these parameters do impact the axial resolution.
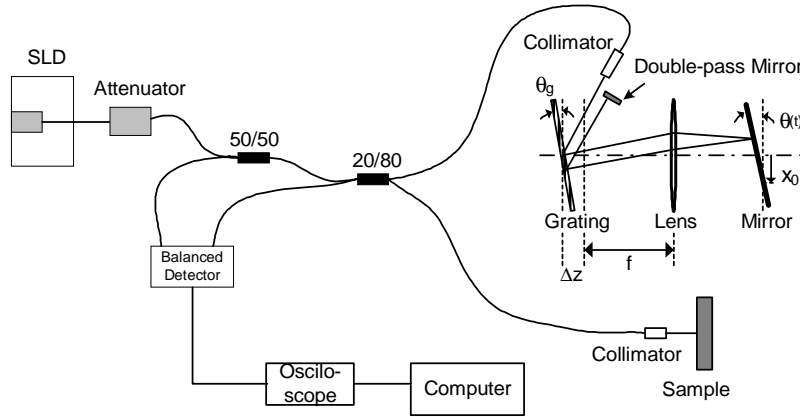

Figure 1. Schematic diagram of a fiber-optic OCT with an FD-ODL in the reference arm.

2. Theory

In order to represent the output signal of the system, we must first start with the input signal, which is the electric field emitted by the source. Given the broadband nature of the light source, it is desirable to express this field by its Fourier components as

$$\mathbf{E}_s(t) = \int_{-\infty}^{\infty} \exp(i\omega t)\hat{\mathbf{E}}_s(\omega)d\omega, \tag{1}$$

where the caret (^) denotes a function in the Fourier domain. Bold letters will denote vectors or matrices. Next, we may express the field at the detector in terms of the field at the source as

$$\mathbf{E}(t) = \int_{-\infty}^{\infty} \alpha_1 \exp[i\phi_1(\omega,t) + i\omega t]\hat{\mathbf{E}}_s(\omega)d\omega +$$
$$\int_{-\infty}^{\infty} \hat{\alpha}_2(\omega)\exp[i\phi_2(\omega,t) + i\omega t]\hat{\mathbf{E}}_s(\omega)d\omega, \tag{2}$$

where the first term is the electric field from the reference arm, and the second term is the electric field from the specimen. Because we use vector field theory, the expression given in Eq. (2) applies to any state of polarization. The

term $\alpha_1 \exp[i\phi_1(\omega,t)+i\omega t]$ contains a real number α_1 that is the relative amplitude at the detector of the wave reflected from the mirror in the FD-ODL, and the phase $\phi_1(\omega,t)$ which accounts for the optical path length to the mirror and the associated phase change along the path. We can use the FD-ODL in the reference arm to induce a phase change, which is a function of frequency. The function $\hat{\alpha}_2(\omega)$ is the amplitude at the detector of the component of the wave backscattered from the specimen at the frequency ω and is determined by the refractive index profile of the specimen. Finally, the term $\phi_2(\omega,t)$ accounts for the optical path length in the specimen arm and the associated phase changes caused for example by reflection, dispersion, and movement of the specimen among other possible effects. If we write

$$m(\omega,t) = \alpha_1 \exp[i\phi_1(\omega,t)] + \hat{\alpha}_2(\omega)\exp[i\phi_2(\omega,t)],\tag{3}$$

then we have

$$\mathbf{E}(t) = \int_{-\infty}^{\infty} m(\omega,t)\exp(i\omega t)\hat{\mathbf{E}}_s(\omega)d\omega.\tag{4}$$

In this expression, both $\mathbf{E}(t)$ and $\hat{\mathbf{E}}_s(\omega)$ are stochastic processes. Because of its broadband nature we assume that the source field $\mathbf{E}_s(t)$ obeys circular Gaussian statistics.[15] This assumption implies that $\mathbf{E}(t)$ is also a Gaussian random process. In particular, the mean source field satisfies $\langle\mathbf{E}_s(t)\rangle = 0,$ and thus $\langle\mathbf{E}(t)\rangle = 0.$

Given that the detector has an integration time of Δt, the detected photocurrent is given by

$$I(t) = \frac{e}{\Delta t}\int_{t-\Delta t}^{t} N(t')dt' = \frac{e}{\Delta t}\int_{-\infty}^{\infty} r(t-t')N(t')dt',\tag{5}$$

where e is the electron charge, and $r(t)$ denotes the time integration window of the detector. In this integral, $N(t)$ is a doubly stochastic Poisson random process representing the photoelectrons produced by the field impinging on the detector. Its mean is then given by

$$\langle\langle N(t)\rangle\rangle = \rho\langle\mathbf{E}^{\dagger}(t)\mathbf{E}(t)\rangle,\tag{6}$$

where ρ is proportional to the detector responsivity and area, and the double angle brackets are used to indicate statistical averages over the two sources of randomness. Therefore, the mean current is given by

$$\langle\langle I(t)\rangle\rangle = \frac{e}{\Delta t}\int_{-\infty}^{\infty} r(t-t')\langle\langle N(t')\rangle\rangle dt'.\tag{7}$$

The expectation in the integrand is given by

$$\langle\langle N(t')\rangle\rangle = \rho\int_{-\infty}^{\infty}\int_{-\infty}^{\infty} m^*(\omega,t')m(\omega',t')\exp[i(\omega'-\omega)t']\langle\hat{\mathbf{E}}_s^{\dagger}(\omega)\hat{\mathbf{E}}_s(\omega')\rangle d\omega d\omega'.\tag{8}$$

We will assume that the source field is a stationary random process and define the scalar autocovariance function of the source field as

$$G(\tau) = \langle\mathbf{E}_s^{\dagger}(t-\tau)\mathbf{E}_s(t)\rangle,\tag{9}$$

The stationarity assumption is related to the stability of the source. This assumption may be relaxed to quasistationarity in order to account for other sources of variation in the source field. The scalar autocovariance function has the property; $G^*(\tau) = G(-\tau)$, which ensures that the Fourier transform $\hat{G}(\omega)$ is real. The expectation $\left\langle \hat{E}^\dagger_s(\omega)\hat{E}_s(\omega') \right\rangle$ from (8) may be expressed by means of the inverse Fourier transform as

$$\left\langle \hat{E}^\dagger_s(\omega)\hat{E}_s(\omega') \right\rangle = \frac{1}{4\pi^2} \int_{-\infty}^{\infty} \int_{-\infty}^{\infty} \exp[-i(\omega't_2 - \omega t_1)]\left\langle \mathbf{E}^\dagger_s(t_1)\mathbf{E}_s(t_2) \right\rangle dt_1 dt_2$$
$$= \frac{1}{4\pi^2} \int_{-\infty}^{\infty} \int_{-\infty}^{\infty} \exp[-i(\omega't_2 - \omega t_1)]G(t_2 - t_1)dt_1 dt_2. \tag{10}$$

By using

$$\omega't_2 - \omega t_1 = \frac{1}{2}(\omega' - \omega)(t_2 + t_1) + \frac{1}{2}(\omega' + \omega)(t_2 - t_1), \tag{11}$$

we can reduce Eq. (10) to

$$\left\langle \hat{E}^\dagger_s(\omega)\hat{E}_s(\omega') \right\rangle = \frac{1}{2\pi} \delta(\omega' - \omega) \int_{-\infty}^{\infty} \exp\left[-i\frac{(\omega' + \omega)}{2}s\right]G(s)ds = \delta(\omega' - \omega)\hat{G}(\omega). \tag{12}$$

Hereafter, $\hat{G}(\omega)$ will be represented as $S(\omega)$ which is the power spectral density of the source.

Inserting $\left\langle \hat{E}^\dagger_s(\omega)\hat{E}_s(\omega') \right\rangle$ into Eq. (8) yields

$$\left\langle\left\langle N(t') \right\rangle\right\rangle = \rho \int_{-\infty}^{\infty} |m(\omega, t')|^2 S(\omega)d\omega. \tag{13}$$

In the integrand we have

$$|m(\omega, t')|^2 = \alpha_1^2 + |\hat{\alpha}_2(\omega)|^2 + 2\alpha_1 \, \mathrm{Re}\{\hat{\alpha}_2(\omega)\exp[-i\phi_1(\omega, t') + i\phi_2(\omega, t')]\}. \tag{14}$$

The last term is the interference term, which is usually the focus of detection. Combining Eq. (13) and Eq. (7) further yields

$$\left\langle\left\langle I(t) \right\rangle\right\rangle = \frac{\rho e}{\Delta t} \int_{-\infty}^{\infty} r(t - t')\left[\int_{-\infty}^{\infty} |m(\omega, t')|^2 S(\omega)d\omega\right]dt'. \tag{15}$$

If we assume that the response time of the detector is instantaneous, i.e. $r(t - t') = \delta(t - t')$, Eq. (15) simplifies to

$$\left\langle\left\langle I(t) \right\rangle\right\rangle = \frac{\rho e}{\Delta t} \int_{-\infty}^{\infty} |m(\omega, t)|^2 S(\omega)d\omega. \tag{16}$$

In order to first quantify the effect of dispersion from the fiber and the FD-ODL, the specimen is taken to be a mirror. We will then introduce the effect of the biological specimen. With the mirror as the specimen, $\hat{\alpha}_2(\omega)$ can be replaced by α_2 in Eq. (14). So filtering out the dc term of the photocurrent signal, the remaining ac term representing the interference may be written as

$$
\begin{aligned}
\langle\langle I_{ac}(t)\rangle\rangle &\propto \int_{-\infty}^{\infty} \text{Re}\{\exp i[\phi_2(\omega,t)-\phi_1(\omega,t)]\}S(\omega)d\omega \\
&\propto \int_{-\infty}^{\infty} \text{Re}[\exp i\Delta\phi(\omega,t)]S(\omega)d\omega,
\end{aligned}
\tag{17}
$$

The phase difference $\Delta\phi(\omega,t)$ can be expanded as a Taylor series as follows

$$
\begin{aligned}
\Delta\phi(\omega,t) &= \phi_2(\omega,t)-\phi_1(\omega,t) \\
&= \omega_0 t_p(t)+(\omega-\omega_0)t_g(t)+D_\omega(t)\frac{(\omega-\omega_0)^2}{2!}+D_\omega^{(1)}(t)\frac{(\omega-\omega_0)^3}{3!},
\end{aligned}
\tag{18}
$$

where ω_0 is the center frequency of the light source, $t_p(t)$ is the phase delay, $t_g(t)$ is the group delay, $D_\omega(t)$ is the first-order group delay dispersion, and $D_\omega^{(1)}(t)$ is the second-order group delay dispersion.

Inserting Eq. (17) into Eq. (18), $\langle\langle I_{ac}(t)\rangle\rangle$ may be expressed as

$$
\langle\langle I_{ac}(t)\rangle\rangle \propto \text{Re}\left[
\begin{array}{c}
\int_{-\infty}^{\infty} S(\omega-\omega_0)\exp[i(D_\omega\frac{(\omega-\omega_0)^2}{2!}+D_\omega^{(1)}\frac{(\omega-\omega_0)^3}{3!})] \\
\times\exp(i\omega_0 t_p)\exp[i(\omega-\omega_0)t_g]d\omega
\end{array}
\right],
\tag{19}
$$

where $S(\omega-\omega_0)$ is the source power spectral density centered at ω_0. It can be observed that Eq. (19) is the inverse Fourier transform of the frequency-domain function given by

$$
\hat{\mathbf{I}}_{\mathbf{ac}}(\omega') \propto S(\omega')\exp[i(D_\omega\frac{\omega'^2}{2!}+D_\omega^{(1)}\frac{\omega'^3}{3!})]\exp(i\omega_0 t_p),
\tag{20}
$$

where $\omega' = \omega-\omega_0$. We shall now apply Eq. (20) to the fiber optic interferometer with an FD-ODL in the reference arm. We first need however to establish some expressions for the phase and group delays, as well as the first- and second-order group delay dispersion associated with the FD-ODL. We updated the expressions derived by Zvyagin and D. Sampson et al.[14] for $t_{p\_odl}(t)$, $t_{g\_odl}(t)$, $D_{\omega\_odl}(t)$, and $D_{\omega\_odl}^{(1)}(t)$ in an FD-ODL for a double-pass system, and added the effect of both the fiber-length mismatch between two arms and the effect of the specimen to the equations of a double-pass FD-ODL as follows, which are given by

$$t_p(t) = t_{p\_odl}(t) + t_{p\_fiber}(t) + t_{p\_sample}(t)$$

$$= \frac{4\Delta z}{c} + \frac{4\Delta\theta(t)x_0}{c} + \frac{2\delta}{c} - \frac{2\Delta d_s}{v_{p\_sample}},$$

(21)

$$t_g(t) = t_{g\_odl}(t) + t_{g\_fiber}(t) + t_{g\_sample}(t)$$

$$= \frac{4\Delta z}{c} + \frac{4\Delta\theta(t)x_0}{c} + \frac{8\pi\theta(t)f}{p\omega_0\cos\theta_g} + \frac{2\delta}{c} - \frac{2\Delta d_s}{v_{g\_sample}},$$

(22)

where p is the grating period (= 1.204 μm), f is the focal length of the lens (= 25 mm), Δz is the axial shift of the grating with respect to the focal plane of the lens, θ_g is the tilt of the grating with respect to the lens, x_0 is the lateral offset of the pivot point of the scanning mirror with respect to the optical axis of the lens, $\Delta\theta(t)$ is the scan angle of the mirror, and c is the speed of light. δ is the potential optical path length mismatch $l_r - l_s$ between the reference arm and the specimen arm, l_r is the optical path length in the reference arm, l_s is the optical path length in the specimen arm up to the specimen surface, and Δd_s is the depth of penetration in the specimen. The mismatch is caused by the implementation challenge in setting equal fiber length in both arms of the interferometer. The phase velocity v_{p_sample} is given by c/n_{p_sample}, and the group velocity v_{g_sample} is given by c/n_{g_sample}, where n_{p_sample} is the mean refractive index of the specimen, and the group velocity index n_{g_sample} is given by $n_{p\_sample} - \lambda(dn_{p\_sample}/d\lambda)$. The overall first- and second-order dispersion equations in the interferometer caused by the FD-ODL, the fiber length mismatch, and the specimen are given by

$$D_\omega(t) = D_{\omega\_odl}(t) + D_{\omega\_fiber}(t) + D_{\omega\_sample}(t)$$

$$= -\frac{16\pi^2 c(\Delta z + f\Delta\theta(t)\tan\theta_g)}{p^2\omega_0^3\cos^2\theta_g} + 2\beta_{2\_fiber}\Delta d - 2\beta_{2\_sample}\Delta d_s,$$

(23)

$$D_\omega^{(1)}(t) = D_{\omega\_odl}^{(1)}(t) + D_{\omega\_fiber}^{(1)}(t) + D_{\omega\_sample}^{(1)}(t)$$

$$= \frac{48\pi^2 c(\Delta z + f\Delta\theta(t)\tan\theta_g)}{p^2\omega_0^4\cos^2\theta_g}(1 + \frac{2\pi c\sin\theta_g}{p\omega_0\cos^2\theta_g}) + 2\beta_{3\_fiber}\Delta d - 2\beta_{3\_sample}\Delta d_s,$$

(24)

where Δd is the fiber length mismatch $d_r - d_s$ between the reference arm and the specimen arm, d_r is the fiber length in the reference arm, d_s is the fiber length in the specimen arm, β_{2_fiber} (= 34.95 fs^2/mm) and β_{2_sample} are the first-order dispersion coefficient of the fiber and the specimen, respectively, and similarly β_{3_fiber} (= 420 fs^3/mm) and β_{3_sample} are the second-order dispersion coefficient of the fiber and the specimen, respectively. In Eq.'s (23) and (24) we define the dispersion in the reference arm to be positive if the reference arm fiber is longer than the specimen arm

fiber (i.e. $\Delta d > 0$). Therefore, the dispersion in the specimen arm, which may be introduced by a specimen, should be negative because $D_\omega(t)$ or $D_\omega^{(1)}(t)$ would be zero if the first-order or second-order dispersion in both arms were the same, i.e. they cancel each other. The FD-ODL is employed to induce negative or positive dispersion in the reference arm depending on Δd and the dispersion characteristics of the specimen to match the total first- or second-order dispersion in the interferometer arms.

In order to determine the amount of axial shift of the grating which induces a first-order dispersion equal to the first-order dispersion imposed by a given fiber-length mismatch in the interferometer arms, we assign zero to β_{2_sample} which means we employ a non-dispersive mirror as the sample. So, from Eq. (23) we see that the first-order dispersion is related to Δz as well as the tilt angle of the mirror $\theta(t)$ which may be a sinusoidal or a triangular function of time in the case where θ_g is nonzero. Therefore, the dispersion would be a time-varying function if the grating tilt angle was non-zero. Compensation of a time-varying dispersion would need a dynamic grating axial shift synchronized to the tilt angle of the mirror which is complicated to accomplish. Hence we set the tilt of the grating θ_g to zero. Therefore, the relation between the amount of axial shift Δz of the grating from the focal plane of a lens and a fiber-length mismatch Δd to make the overall first-order dispersion $D_\omega(t)$ zero is given by

$$\frac{\Delta z}{\Delta d} = \frac{\beta_{2\_fiber} p^2 \omega_0^3}{8\pi^2 c}. \qquad (25)$$

Thus, the axial shift Δz required to remove the first-order dispersion caused by the fiber-length mismatch Δd can be set according to the first order dispersion coefficient of the fiber β_{2_fiber}, the grating period p, and the center frequency of the source ω_0, all known or measurable parameters. Therefore, the ratio provided by Eq. (25) may be computed, and if either one of the two parameters Δz or Δd was known, the other could then be determined. In practice, Δz can be theoretically established and Δd can then be computed using Eq. (25).

3. Results

We implemented the fiber optic interferometer shown in Figure 1 first with a mirror as sample. A superluminescent diode (SLD-47HP Superlum Diodes) centered at 950 nm with a spectral bandwidth of approximately 70nm and a power of 7mW illuminated the interferometer. An attenuator was employed to prevent optical feedback into the SLD, which would cause permanent damage to the source. A circulator or isolator centered at 950nm and of large bandwidth would have been preferred but such components are not yet commercially available. The light emitted by the SLD went through two fused fiber couplers. A splitting ratio of 80/20 enabled transmission of maximum power into the specimen reducing the excess noise arising from the reference arm. Figure 1 also shows the FD-ODL that was used for depth scanning and dispersion compensation. We used a balanced detector (Nirvana 2017) connected to a real-time oscilloscope (Tektronix TDS210) in order to observe the photocurrent signal. The oscilloscope was connected to a computer which was employed to record the signal.

We used the given values for parameters in Eq. (25) and obtained the ratio $\Delta z / \Delta d = 0.0168$. The grating was set to be parallel to the lens so that the tilt angle of the grating was zero. To obtain the narrowest photocurrent signal we shifted the grating axially in order to match the first-order dispersion in the arms of the fiber optic interferometer. We then simulated the photocurrent signal of the system by theoretically varying Δz and x_0. The value of x_0 validated theoretically, was set experimentally at 0.4mm. Such value enforces a low modulation frequency of the photocurrent signal, which is directly proportional to x_0 as shown in Eqs. (20) and (21). Δz was set at 0.06mm and validated theoretically as well. The fiber-length mismatch Δd was then computed to be 3.6 mm using Eq. (25). Fig. 2(a) shows the narrowest photocurrent signal obtained experimentally by adjusting the grating axial shift Δz to compensate the first-order dispersion induced by the fiber-length mismatch. Fig. 2(b) represents the corresponding photocurrent signal

simulated using $\Delta z = 0.06$ mm, $\Delta d = 3.6$ mm, and $x_0 = 0.4$ mm. These figures explain that the first-order dispersion induced by $\Delta z = 0.06$ mm compensates the first-order dispersion induced by the 3.6mm of fiber-length mismatch between the two arms. Under such setting, there remains no overall first-order dispersion. However, the second-order dispersion corresponding to $\Delta z = 0.06$ mm and $\Delta d = 3.6$ mm is non zero and is best shown by the asymmetric small oscillations in Figs. 2(a-b).
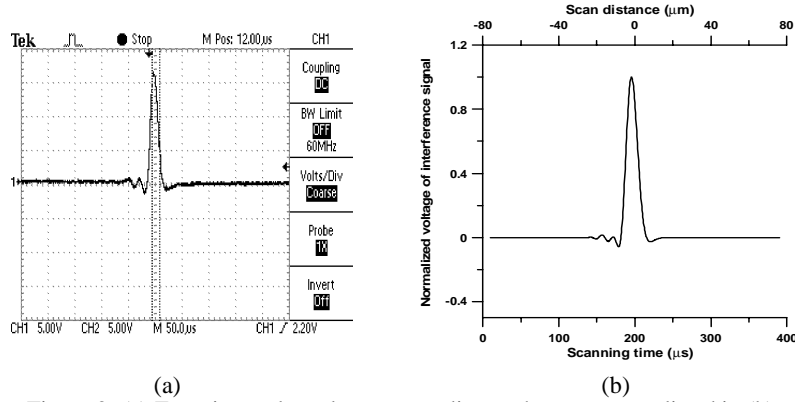

(a) (b)

Figure 2. (a) Experimental result corresponding to the parameters listed in (b);
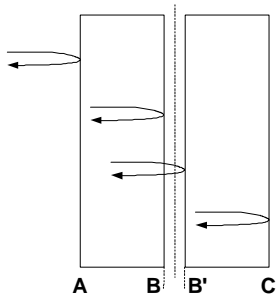(b) Simulation result for $\Delta z = 0.06$ mm, $\Delta d = 3.6$ mm, and $x_0 = 0.4$ mm.

Figure 3. LiTaO$_3$
layers

In the first experiment the sample employed was a mirror which is assumed to be non-dispersive. To observe the impact of a dispersive specimen we replaced the mirror with a sample consisting of two 0.5 mm thick LiTaO$_3$ plates separated by an air gap of ~80 μm as depicted in Figure 3. We chose LiTaO$_3$ since it has comparable dispersion characteristics with skin, which is a common specimen we employ in OCT imaging. The first and second order dispersion coefficients of LiTaO$_3$ are 236.8 fs^2/mm and 188 fs^3/mm, where the ones of skin are 109 fs^2/mm (about the half of LiTaO$_3$'s) and 159 fs^3/mm, respectively.

We created three scenarios with our LiTaO$_3$ specimen to demonstrate the effect of dispersion manipulation with FD-ODL on the photocurrent signal and acquired images. The first scenario presented in Figure 4(a) shows the photocurrent signal recorded scanning through the line S in Figure 4(b) when the first-order dispersion was compensated for the light reflected from the layer A in Figure 3. The 2-D image of the specimen is shown in Figure 4(b). For the light reflected from the back-end of LiTaO$_3$ which is layer C, the impact of dispersion is so severe that the corresponding photocurrent signal is broadened maximally.

We investigated a second scenario where the grating of the FD-ODL was moved closer to the lens of the FD-ODL, i.e. Δz was decreased, so that the total first-order dispersion in the system was zero for the light reflected in the mid-plane of LiTaO$_3$ plates. We computed the corresponding grating axial shift to be 0.005 mm. Figure 4(c) and (d) present the measured photocurrent signals resulting from reflections off layers A, B, and C, respectively and the OCT image of the specimen. In this case, results show a lessened overall broadening of the photocurrent signal envelopes across the depth of the specimen and a weaker effect of first-order dispersion in the photocurrents. The photocurrent signal less affected by the first order dispersion is naturally the one detected from layer B.

To be comprehensive, we investigated a final scenario, where we further decreased the grating axial shift Δz down to -0.055 mm so that the total first-order dispersion was set to zero for the light reflected from the layer C in Figure 3. The severe impact of the first-and second-order dispersion is demonstrated in Fig. 4(e), along with the image in the Figure 4(f), for the photocurrent signal resulting from the reflection off layer A of the specimen.

Table 1 presents the computed axial resolutions of each isolated lobe in the photocurrent signals in Figure 4. ASI stands for absolute-square-integral of the photocurrent signal with respect to scan distance and RMSW is the root-mean-

square-width. We omit the full-width at half-maximum (FWHM) metric because of the asymmetrical shape of photocurrent signals due to dispersion in the system.

Table 1. Computed axial resolutions

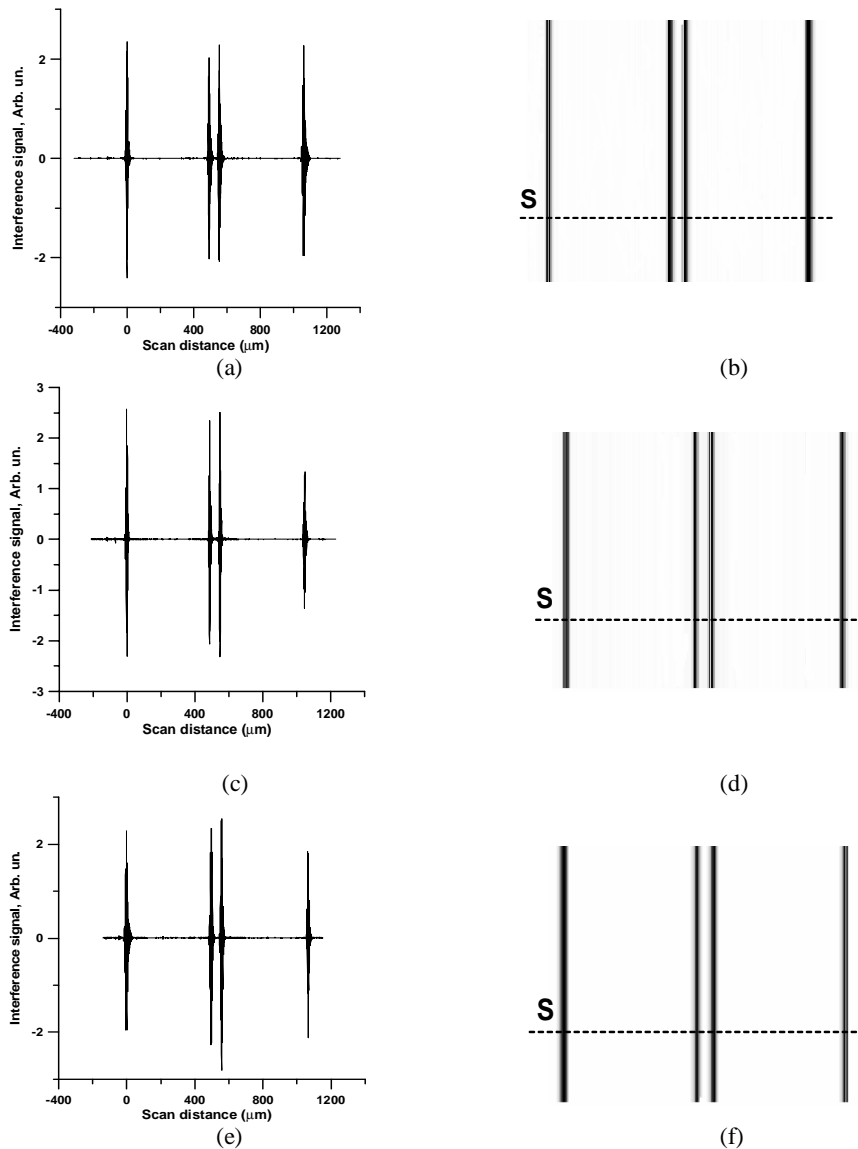| Case	Metric	l_A (µm)	l_B (µm)	$l_{B'}$ (µm)	l_C (µm)
Front surface	ASI	6.35	8.04	8.04	14.23
dispersion compensation	RMS-width	8.87	12.94	12.94	18.71
Middle surface	ASI	8.05	6.18	6.18	8.16
dispersion compensation	RMS-width	12.67	8.05	8.05	12.14
Back surface	ASI	14.45	8.25	8.25	6.00
dispersion compensation	RMS-width	18.34	11.96	11.96	7.33

Figure 4. (a) First-order dispersion compensated for the signal reflected off the surface A in Fig. 3. and (b) image of the layers; (c) first-order dispersion compensated for the signal reflected off the surface B in Fig. 3. and (d) image of the layers; (e) First-order dispersion compensated for the signal reflected off the surface C in Fig. 3. and (f) image of the layers

4. Conclusion

In this paper, we demonstrated the impact of dispersion up to second-order in a fiber-optic interferometer that has the general structure of an OCT system. The dispersion effects induced by $LiTaO_3$ were included for its similarity of dispersion characteristics to skin specimens. We presented a theoretical and associated experimental framework for minimizing broadening of the envelopes of the photocurrent signals observed across the depth of the specimen. We quantified how first-order dispersion in the overall system with a biological specimen can be compensated by employing an FD-ODL with a grating with variable axial position. Studies and results showed that the second-order dispersion cannot be compensated together with the first-order dispersion. However we proposed a dispersion compensation method for highest overall axial resolution across the depth of the specimen. Particularly, the method proposed is suitable for imaging a few millimeters into depth into the specimen. Specifically, if the overall first-order dispersion compensation is set for the photocurrent signal resulting from the light reflected from around the middle plane of the specimen, the impact of first-order dispersion on the photocurrent signal is overall minimized and resolution is highest across the depth of the specimen.

Acknowledgements

References

1. D. Huang, E. A. Swanson, C. P. Lin, J. S. Schuman, W. G. Stinson, W. Chang, M. R. Hee, T. Flotte, K. Gregory, C. A. Pulifito, and J. G. Fujimoto, "Optical coherence tomography," Science **254**, 1178-1181 (1991).
2. G. J. Tearney, B. E. Bouma, S. A. Boppart, B. Golubovic, E. A. Swanson, and J. G. Fujimoto, "Rapid acquisition of in vivo biological images by use of optical coherence tomography," Optics Letters **21**, 1408-1410 (1996).
3. A. M. Rollins, M. D. kulkarni, S. Yazdanafar, R. Ungarunyawee, and J. A. Izatt, "In vivo video rate optical coherence tomography," Optics Express **3**, 219-229 (1998), http://www.opticsexpress.org.
4. D. L. Marks, A. L. Oldenburg, J. J. Reynolds, and S. A. Boppart, "Digital Algorithm for Dispersion Correction in Optical Coherence Tomography for Homogeneous and Stratified Media," Appl. Opt. **42**, 204-217 (2003).
5. A. F. Fercher, C. K. Hitzenberger, M. Sticker, and R. Zawadzki, "Numerical dispersion compensation for Partial Coherence Interferometry and Optical Coherence Tomography," Optics Express **9**, 610-615 (2001), http://www.opticsexpress.org.
6. D. L. Marks, A. L. Oldenburg, J. J. Reynolds, and S. A. Boppart, "Autofocus Algorithm for Dispersion Correction in Optical Coherence Tomography," Appl. Opt. **42**, 3038-3046 (2003).
7. R. A. Leitgeb, W. Drexler, A. Unterhuber, B. Hermann, T. Bajraszewski, T. Le, A. Stingl, and A. F. Fercher, "Ultrahigh resolution Fourier domain optical coherence tomography," Optics Express **12**, 2156-2165 (2004).
8. M. Wojtkowski, V. J. Srinivasan, T. H. Ko, J. G. Fujimoto, A. Kowalczyk, and J. S. Duker, "Ultrahigh-resolution, high-speed, Fourier domain optical coherence tomography and methods for dispersion compensation," Optics Express **12**, 2404-2422 (2004).
9. B. Cense, N. A. Nassif, T. C. Chen, M. C. Pierce, S. Yun, B. H. Park, B. E. Bouma, G. J. Tearney, and J. F. de Boer, "Ultrahigh-resolution high-speed retinal imaging using spectral-domain optical coherence tomography," Optics Express **12**, 2435-2447 (2004).
10. E. D. J. Smith, A. V. Zvyagin, and D. D. Sampson, "Real-time dispersion compensation in scanning interferometry," Optics Letters **27**, 1998-2000 (2002).
11. K.F. Kwong, D. Yankelevich, K.C. Chu, J.P. Heritage, and A. Dienes,"400-Hz mechanical scanning optical delay line," Optics Letters **18**, 558-561 (1993).
12. G. J. Tearney, B. E Bouma, and J. G. Fujimoto, "High speed phase- and group-delay scanning with a grating based phase control delay line," Optics Letters **22**, 1811-1812 (1997).

13. W. K. Niblack, J. O. Schenk, B. Liu, and M. E. Brezinski, "Dispersion in a Grating-Based Optical Delay Line for Optical Coherence Tomography," Appl. Opt. **42**, 4115-4118 (2003).
14. A. V. Zvyagin, E. D. J. Smith, and D. D. Sampson, "Delay and dispersion characteristics of a frequency-domain optical delay line for scanning interferometry," J. Opt. Soc. Am. A **20**, 333-341 (2003).
15. H. H. Barrett, and K. J. Myers, B.E.A. Saleh. Ed., *Foundations of Image Science*, (Wiley Series in Pure and Applied Optics, Hoboken, New Jersey, 2004).